Compliance and frequency optimization for energy efficiency in cyclic tasks

Mohammad Shushtari†, Rezvan Nasiri†*,
Mohammad Javad Yazdanpanah‡ and
Majid Nili Ahmadabadi†

†Cognitive Systems Laboratory, Control and Intelligent Processing Center of
Excellence (CIPCE), School of Electrical and Computer Engineering, College of Engineering,
University of Tehran, Tehran, Iran.
E-mails: nasiri.rezvan@gmail.com, sm.shushtari@gmail.com, mnili@ut.ac.ir
‡Advanced Control Systems Laboratory, Control and Intelligent Processing
Center of Excellence (CIPCE), School of Electrical and Computer Engineering,
College of Engineering, University of Tehran, Tehran, Iran.
E-mail: yazdan@ut.ac.ir

SUMMARY
We present an analytical method for the concurrent calculation of optimal parallel compliant elements and frequency of reference trajectories for serial manipulators performing cyclic tasks. In this approach, we simultaneously shape and exploit the robot's natural dynamics by finding a set of compliant elements and task frequency that result in minimization of an energy-based cost function. The cost function is the integral of a weighted squared norm of the generalized forces. We prove that the generalized force needed for tracking the reference trajectory is a linear function of compliance coefficients and a quadratic function of task frequency. Therefore, the cost function is quadratic with respect to stiffness coefficients and quartic with respect to the task frequency. These properties lead to a well-posed optimization problem with a closed-form solution. Using three case studies, we elucidate the properties of our method.

KEYWORDS: Energy efficiency; Optimum compliance; Optimum Frequency; Cyclic tasks; Natural dynamics.

1. Introduction
Many robotic tasks include cyclic motions; major examples are pick-and-place tasks and legged locomotion. The periodic nature of cyclic motions can be potentially exploited to increase energy efficiency. Nevertheless, in industrial robots, this potential is not sufficiently used since an energy source is easily available in industrial environments. However, other strategies, like reducing the weight of robots, are widely used in the industry. In contrast, in legged locomotion, intensive attention to all possible means for increasing energy efficiency, including exploiting the cyclic nature of walking, is necessary due to limited capacity of legged robots in carrying their energy supply.

Broadly speaking, the existing researches about using the cyclic nature of tasks for energy efficiency can be divided into two broad categories: *Natural Dynamics Modification (NDM)* and *Natural Dynamics Exploitation (NDE)*. The first category includes researches on robots' bodies aimed at decreasing energy consumption. These studies mainly employ two types of methods. In the first type, the robot's whole body is designed to perform a given periodic task efficiently (see refs. [5,11,24,30]) while in the second type, some specific parts of the robot's body are tuned or adapted

* Corresponding author. E-mail: nasiri.rezvan@gmail.com

(see refs. [1,8,10,16,22,24–31]). Although the first set of methods results in more efficient robots for a given task, their application is restricted. This happens because in many cases, a robot should perform multiple tasks and changing its whole body over the tasks is costly or even impossible. In contrast, changing or adapting simple but more effective parts of the robots for achieving energy efficiency per task is doable; see [16].

Compliant elements, with simple installation at joints, are appropriate candidates for decreasing energy consumption in cyclic tasks. Such elements appear in two different configurations: serial and parallel. Both configurations provide room for natural dynamic modification and lowering energy consumption; see refs. [10,16,22,31] as examples of using parallel elastic actuators [refs. 8,33,34], as examples of using serial elastic actuators, and [ref. 6] for a comparison between these two. Nevertheless, the parallel configuration is more favored due to the facts that, unlike the serial one, a parallel compliance does not enlarge the robot's configuration space and has a well-posed quadratic cost function for energy consumption minimization with respect to the compliance coefficients; see ref. [16].

The optimal parallel compliance can be found either in *offline* or *online* manners. Online adaptation of compliant elements is more beneficial in the case of frequently varying tasks and system dynamics; see refs. [31,16]. However, it requires more efforts on variable compliance design, employing sensory feedback, and actuating the compliance. On the other hand, offline methods are more applicable for predefined and scheduled tasks and systems.

While the NDM methods reduce energy consumption by manipulation of the robot's structure, the NDE approaches alter the robot's motion to achieve efficiency (see ref. [27] as an example). This alteration is done by exploring the feasible trajectory space. Redundancy resolution is one of the NDE methods which provides energy efficient joints trajectories by searching in the null-space of redundant robots; see ref. [18]. Another approach is to use a reference trajectory generated by biological or mechanical structures; e.g., animals or passive walkers; see refs. [13 and 14]. This approach is based on this assumption that such trajectories are optimum for that specific structures. CPG (Central Pattern Generator) oscillators provide us with an adaptive tool to learn periodic reference trajectories; see refs. [7,19,25]. It is shown in some examples that CPGs can synchronize the reference trajectory with the resonant frequency of the robot which consequently results in energy efficiency. However, there are no proofs of convergence and optimality for this method in general; see refs. [3 and 7]. In addition, DMP (Dynamic Movement Primitives) is another approach which improves a given task to satisfy an objective function (e.g., energy consumption); see ref. [20].

In our previous works [refs. 9,15], we introduced two adaptive oscillators with linear and non-linear dynamical equations (ANO and NANO) to tune the frequency and the shape of the cyclic motions for energy efficiency. In contrast with CPG and DMP, our oscillators have optimality and convergence proofs for 1-DOF robotic joints.

In this paper, we develop an analytical and offline method to benefit from both possibilities, NDE and NDM, for energy consumption minimization. That is, we concurrently calculate both the optimum compliances at the joints and the frequency of the reference trajectory which result in maximum energy efficiency. In doing so, we consider the dynamical model of a serial manipulator and compute the optimum parameters in an analytical closed-form manner. In our method, compliant elements are non-linear and are in the parallel configuration. Interestingly, based on ref. [29], dynamical equations of a legged robot, except in some limited intervals (as "instant double support"), are compatible with a manipulator. Hence, without loss of generality, the presented method can be applied to both manipulators and legged robots in order to optimize the compliances and the task frequency.

The rest of the paper is organized as follows: the problem is stated in Section 2. The mathematical analyses are presented in Section 3. In Section 4, three case studies are presented to give a tangible insight of the approach. Conclusions and discussions are given in the last section.

2. Problem Statement and Definitions

Consider an n-DOF robotic manipulator which conforms with the following continuous dynamical equation:

$$\mathbf{M}(\mathbf{q})\ddot{\mathbf{q}} + \mathbf{C}(\mathbf{q}, \dot{\mathbf{q}})\dot{\mathbf{q}} + \mathbf{G}(\mathbf{q}) = -\mathbf{F}_c(\mathbf{q}) - \mathbf{B}\dot{\mathbf{q}} + \mathbf{u}, \tag{1}$$

where $\mathbf{u} \in \mathbb{R}^n$ is the vector of actuator forces/torques, $\mathbf{q}, \dot{\mathbf{q}}, \ddot{\mathbf{q}} \in \mathbb{R}^n$ are the vectors of joint positions, velocities and accelerations, respectively, $\mathbf{M}(\mathbf{q}) \in \mathbb{R}^{n \times n}$ is the positive-definite inertia matrix, $\mathbf{C}(\mathbf{q}, \dot{\mathbf{q}}) \in \mathbb{R}^{n \times n}$ denotes the centrifugal and Coriolis forces, $\mathbf{G}(\mathbf{q}) \in \mathbb{R}^n$ denotes forces due to the gravity, $\mathbf{F}_c(\mathbf{q}) \in \mathbb{R}^n$ is the vector of parallel compliance forces/torques, and $\mathbf{B} = diag(b_1, b_2, \ldots, b_n)$ is the positive-definite viscosity matrix where $b_1, b_2, \ldots, b_n \in \mathbb{R}^+$ are the viscosity coefficients. Equation (1) is assumed to be well known.

Through the text, we consider the following points:

1. For the sake of simplicity, we forbear specifying the argument of dynamical equation elements except where required.
2. $\mathbf{A}_i$ represents the ith element of the vector $\mathbf{A}$ and $\mathbf{A}_{ij}$ represents the element of ith row and jth column of the matrix $\mathbf{A}$.

Definition 1 (Parallel compliance force/torque). The parallel compliance force at the ith joint is defined as

$$f_{ci}(\mathbf{q}_i) = \sum_{j=1}^m k_{ij}\phi_{ij}; \ \forall \begin{cases} i = 1, \ldots, n \\ j = 1, \ldots, m, \end{cases} \tag{2}$$

where $\phi_{ij} = \phi_j(\mathbf{q}_i)$ and k_{ij} are the jth basis function and compliance coefficient of the ith joint, respectively.

The compliance coefficients are all considered as free parameters which are left to be optimized along with the task frequency. Note that by proper selection of the basis functions (ϕ_j), this definition represents any compliance force profile (e.g., a set of polynomial basis functions [17, pp. 233]). Nevertheless, the production constraints should be considered in defining the basis functions (see refs. [2,14,21,23] as examples for non-linear compliance design). Based on this definition, the vector of compliant forces ($\mathbf{F}_c(\mathbf{q})$) is represented as $\mathbf{F}_c(\mathbf{q}) = [f_{c1}, f_{c2}, \ldots, f_{cn}]^T$.

Definition 2 (Inverse kinematics solution). There exists a sufficiently smooth and bijective mapping between task-space ($\mathbf{X} \subset \mathbb{R}^p$) and joint-space ($\mathbf{Q} \subset \mathbb{R}^n$) as

$$\mathbf{q} = \mathbf{T}(\mathbf{x}) \, ; \mathbf{T} : \mathbf{X} \to \mathbf{Q} \ ; \ \mathbf{x} \in \mathbf{X} \, , \ \mathbf{q} \in \mathbf{Q}.$$

Note that this mapping is not necessarily unique (see Section 5.1).

According to the presented definition, any kind of control objectives can be easily included in the task space; e.g., the end-effector's position and orientation.

Definition 3 (Robot's task). The robot's task is to periodically move in the task space ($\mathbf{X}$) on sufficiently smooth and non-self-crossing closed curves $\mathbf{r} = \mathbf{R}(\theta) \, ; \mathbf{R} : \mathbb{R} \to \mathbf{X}$. Here, $\mathbf{R}$ is periodic with respect to θ and it is defined in such a way that the robot never gets singular.

Definition 4 (Task frequency). By defining $\omega \in \mathbb{R}^+$ as the task frequency, we have $\theta(t) = \omega t$. In this paper, ω is a time-invariant free parameter which is left to be optimized.

Based on Definitions 2–4, the reference joint trajectory is

$$\mathbf{q}_r(\omega t) = \mathbf{T}(\mathbf{R}(\omega t)). \tag{3}$$

Definition 5 (Cost function). The cost function is

$$W = \int_0^{2\pi} \mathbf{u}^T \mathbf{N} \mathbf{u} \, d\theta = \omega \int_0^{\frac{2\pi}{\omega}} \mathbf{u}^T \mathbf{N} \mathbf{u} \, dt, \tag{4}$$

where $\mathbf{N} \in \mathbb{R}^{n \times n}$ is a positive-definite weighting matrix.

The presented cost function is proportional to the total energy consumption when DC-motors are employed for actuation of the joints.

3. Mathematical Analysis

3.1. Desired forces/torques extraction

To extract the desired forces/torques, we find $\mathbf{u}$ such that $\ddot{\mathbf{q}} = \ddot{\mathbf{q}}_r$, $\dot{\mathbf{q}} = \dot{\mathbf{q}}_r$, and $\mathbf{q} = \mathbf{q}_r$; where $\mathbf{q}_r$ is the reference trajectory. Hence, based on Eq. (1), we have

$$\mathbf{u} = \mathbf{M}(\mathbf{q}_r)\ddot{\mathbf{q}}_r + \mathbf{C}(\mathbf{q}_r, \dot{\mathbf{q}}_r)\dot{\mathbf{q}}_r + \mathbf{G}(\mathbf{q}_r) + \mathbf{F}_c(\mathbf{q}_r) + \mathbf{B}\dot{\mathbf{q}}_r. \tag{5}$$

Theorem 1 (Transformed desired forces/torques). By considering the stated assumptions and definitions, the desired forces/torques are transformed as

$$\mathbf{u} = \omega^2 \Psi(\omega t) + \omega \mathbf{B}\mathbf{q}'_r(\omega t) + \mathbf{G}(\mathbf{q}_r(\omega t)) + \mathbf{F}_c(\mathbf{q}_r(\omega t)), \tag{6}$$

where $\Psi(\omega t) = [\psi_1(\omega t), \psi_2(\omega t), \ldots, \psi_n(\omega t)]^T$ and $\psi_i(\omega t)$ is

$$\psi_i(\omega t) = \sum_{j=1}^{n} ((\mathbf{M}_{ij}(\mathbf{q}_r)\mathbf{q}''_{r_j})$$

$$+ \frac{1}{2}\mathbf{q}'_{r_j}(\omega t) \sum_{k=1}^{n} (\frac{\partial \mathbf{M}_{ij}(\mathbf{q}_r)}{\partial \mathbf{q}_{r_j}} + \frac{\partial \mathbf{M}_{ik}(\mathbf{q}_r)}{\partial \mathbf{q}_{r_j}} - \frac{\partial \mathbf{M}_{kj}(\mathbf{q}_r)}{\partial \mathbf{q}_{r_i}})\mathbf{q}'_{r_k}(\omega t))$$

Also, we have $\mathbf{q}'_r(\omega t) = \frac{\partial \mathbf{q}_r(\omega t)}{\partial(\omega t)}$ and $\mathbf{q}''_r(\omega t) = \frac{\partial^2 \mathbf{q}_r(\omega t)}{\partial(\omega t)^2}$.
See Appendix A for proof.

3.2. Cost function optimization

Based on Eq. (6), $\mathbf{u}^T \mathbf{N}\mathbf{u}$ is calculated as

$$\mathbf{u}^T \mathbf{N}\mathbf{u} = \omega^4 \Psi^T \mathbf{N}\Psi + 2\omega^3 \Psi^T \mathbf{N}\mathbf{B}\mathbf{q}'_r + \omega^2 (2\Psi^T \mathbf{N}(\mathbf{G} + \mathbf{F}_c) + \mathbf{q}'^T_r \mathbf{B}\mathbf{N}\mathbf{B}\mathbf{q}'_r) \tag{7}$$

$$+ 2\omega \mathbf{q}'^T_r \mathbf{B}\mathbf{N}(\mathbf{G} + \mathbf{F}_c) + (\mathbf{G} + \mathbf{F}_c)^T \mathbf{N}(\mathbf{G} + \mathbf{F}_c).$$

By substituting Eq. (7) into Eq. (4), we have

$$W = \alpha_4 \omega^4 + \alpha_3 \omega^3 + \omega^2 (\alpha_2 + \sum_{i=1}^{n} \sum_{j=1}^{m} \gamma_{ij} k_{ij}) + \omega(\alpha_1 + \sum_{i=1}^{n} \sum_{j=1}^{m} \lambda_{ij} k_{ij})$$

$$+ \alpha_0 + \sum_{i=1}^{n} \sum_{j=1}^{m} \xi_{ij} k_{ij} + \sum_{i=1}^{n} \sum_{j=1}^{m} \sum_{l=1}^{n} \sum_{s=1}^{m} \zeta_{ijls} k_{ij} k_{ls}, \tag{8}$$

where α_p ($p = 0, \ldots, 4$), $\gamma_{ij}, \lambda_{ij}, \xi_{ij}$, and ζ_{ijls} ($i, l = 1, \ldots, n$, $j, s = 1, \ldots, m$) are constant values (see Appendix B for the detailed calculations). According to Eq. (8), the cost function is a quadratic function with respect to the compliances coefficients (k_{ij}) and is quartic with respect to the task frequency (ω). By exploiting this property, we compute the optimum values of these free parameters ($\mathbf{z}^*$) analytically as

$$\mathbf{z}^* = \arg \min_{\mathbf{z}} W(\mathbf{z}); \ \mathbf{z} = [k_{11}, \ldots, k_{1m}, \ldots, k_{n1}, \ldots, k_{nm}, \omega]^T$$

subject to $\omega \geqslant 0$.

Principally, we are facing a constrained optimization problem here. Relaxing the constraint, we can find $\mathbf{z}^*$:

$$\frac{\partial W(\mathbf{z})}{\partial \mathbf{z}}|_{\mathbf{z}=\mathbf{z}^*} = 0 \quad \& \quad \frac{\partial^2 W(\mathbf{z})}{\partial \mathbf{z}^2}|_{\mathbf{z}=\mathbf{z}^*} > 0. \tag{9}$$

In case of $\omega^* \leq 0$, we infer that there is no optimum frequency for the given task.

3.3. Effect of precompression on the optimization process

Maximization of Eq. (8) in different situations may result in non-zero optimum frequencies; see Section 4 for some examples. This may raise this question: Why moving on the desired path is more efficient than holding a particular position? To answer this question, we should note that the rest lengths of the compliant elements are predefined, and the equilibrium points of the manipulator may not be on the desired path. Therefore, moving with an optimum non-zero frequency can be more energy efficient than staying idle on the path. Now, by adding some constants to the basis functions, we include the rest lengths of the compliant elements to the list of free parameters for the optimization. Adding the rest lengths provides the possibility of having precompression in the compliances. In this case, in Eq. (1), $\mathbf{F}_c$ is modified as follows:

$$\mathbf{F}_c(\mathbf{q}) = \hat{\mathbf{F}}_c(\mathbf{q}) + \mathbf{F}_0; \hat{\mathbf{F}}_c(\mathbf{0}) = \mathbf{0}.$$

Applying this modification to the optimization process results in zero optimum frequency and optimal cost function ($\omega^* = 0$, $W^* = 0$), for all coefficients of the basis functions. Interestingly, the optimum rest length is calculated as $F_0 = -G(0)$. In other words, by adding the precompression in the set of basis functions, this degree of freedom is utilized to create an equilibrium point on the desired path.

Clearly, according to Section 3, $\omega^* = 0$ is in contradiction with our assumption on the acceptable frequencies ($\omega > 0$). To deal with this problem, here we change the constraint on the acceptable frequencies to $\omega \geq \omega_0$.

Henceforth, we should solve Eq. (8) as a constraint optimization problem, taking precompressions into account. First, assume that the constraint is inactive, which results in $\omega^* = 0$ and $W^* = 0$. This is the only global optimum frequency of the cost function based on its quartic form. In addition, the obtained result is in contradiction with the assumed constraint ($\omega^* \geq \omega_0$). Hence, we can conclude that the assumed constraint is active and $\omega^* = \omega_0$ is the global optimum frequency. Consequently, the optimum compliance coefficients including precompressions are obtained by substituting $\omega = \omega_0$ in Eq. (8) and minimizing the resultant cost function.

3.4. Sensitivity of the cost function to model inaccuracy

In Section 2, we assumed that the parameters of the model are known. Although these parameters could be obtained using system identification methods with high precision, a narrow band of the parameter-estimation-error is inevitable. Also, some parameters of the system usually change with aging. Therefore, we study the effect of deviation from nominal model parameters on the optimal value of the cost function.

Consider β as an uncertain parameter of the model with nominal value β_0 and $\beta = \beta_0 + \Delta\beta$. Based on the presented method in Section 3.2 and using *Taylor* series, in a relatively small vicinity of β_0, we have

$$W^*(\beta) = W^*(\beta_0) + \frac{\partial W^*(\beta)}{\partial \beta}\big|_{\beta=\beta_0}\Delta\beta + O(\Delta\beta),$$

where $lim_{\Delta\beta \to 0} \frac{O(\Delta\beta)}{\Delta\beta} = 0$.

Defining $\Delta W^*(\beta_0) \triangleq \frac{\partial W^*(\beta)}{\partial \beta}\big|_{\beta=\beta_0}\Delta\beta$, we have

$$W^*(\beta) \approx W^*(\beta_0) + \Delta W^*(\beta_0).$$

Considering $S(\beta_0) \triangleq \Delta W^*(\beta_0)/W^*(\beta_0)$ as a sensitivity factor, we obtain an intuition about the sensitivity of the presented method in the vicinity of nominal model parameters. In other words, less sensitivity factor means that the presented method can find the optimum frequency and compliance coefficients in a wider vicinity of nominal parameters of the system.

3.5. Dealing with model uncertainty

Having a *complete model* might seem a strong assumption since unmodeled dynamics are unavoidable. Here, we relax this assumption and include the effects of parametric uncertainties in the dynamical model. In case of stochastic uncertainty in the model parameters, each related term in the cost function

(α_i, λ_{ij}, γ_{ij}, ξ_{ij}, and ζ_{ijls} in Eq. (8)) comes from a stochastic distribution. Therefore, we minimize the expected value of the cost function; i.e.,

$$E(W) = E(\alpha_4)\omega^4 + E(\alpha_3)\omega^3 + \omega^2(E(\alpha_2) + \sum_{i=1}^{n}\sum_{j=1}^{m} E(\gamma_{ij})k_{ij})$$

$$+ \omega(E(\alpha_1) + \sum_{i=1}^{n}\sum_{j=1}^{m} E(\lambda_{ij})k_{ij}) + E(\alpha_0)$$

$$+ \sum_{i=1}^{n}\sum_{j=1}^{m} E(\xi_{ij})k_{ij} + \sum_{i=1}^{n}\sum_{j=1}^{m}\sum_{l=1}^{n}\sum_{s=1}^{m} E(\zeta_{ijls})k_{ij}k_{ls},$$

where E is the expectation operator. The process of computing the optimum frequency and the compliance coefficients for this cost function is exactly the same as in Eq. (8).

3.6. Multiple tasks optimization

Our method is model-based and works offline. Therefore, it is applicable when a single or a defined set of cyclic tasks are repeatedly performed for a sufficiently extended period of time. In multi-task cases where changing the compliant elements over tasks is not feasible, the cost function is a weighted sum of the original cost functions defined over the tasks (Eq. (8)). The following equation represents the unified cost function:

$$W_u = \sum_{i=1}^{d} C_i W_i \; ; \; \sum_{i=1}^{d} C_i = 1,$$

where W_u is the unified cost function, W_i is the cost function for each task, d is the number of tasks, and C_i is the positive weight value for each task. Computation of the optimum frequency and compliance coefficients is exactly the same as in Section 3.2.

4. Case Studies

In this section, first we apply the presented optimization method on a simple 2-DOF prismatic serial manipulator where the whole procedure could be easily followed due to the simplicity of the system and the calculations. Also, the effect of adding extra basis functions to the compliance profile is studied. Then, we apply the method on a two-link manipulator with rotary joints and finally, to show the applicability and generality of our method, we consider a RRP manipulator performing a 3D task with multi-basis compliances at its joints. The simulations are performed using MATLAB/Simulink/Simmechanis.[12]

In the simulations, the dimension of frequency is [rad/s], the dimension of linear compliance in rotary joints is [Nm/rad], the dimension of cubic compliance in rotary joints is [Nm/rad^3], the dimension of linear compliance in prismatic joints is [N/m], and the dimension of cubic compliance in prismatic joints is [N/m^3].

4.1. 2-DOF manipulator with prismatic joints

Consider a two-link planar manipulator with compliant prismatic joints (Fig. 1a). In this setup, for the sake of simplicity, the mass of links is neglected in comparison with the mass of end-effector. The manipulator's dynamical equations are

$$\begin{cases} m\ddot{x} + f_x(x) + b_x\dot{x} = u_x \\ m\ddot{y} + f_y(y) + b_y\dot{y} = u_y, \end{cases}$$

where m is the end-effector mass, b_x and b_y are the damping coefficients in x and y directions, respectively. Considering $\phi_{x1} = x$, $\phi_{x3} = x^3$, $\phi_{y1} = y$, and $\phi_{y3} = y^3$, the compliance forces are

$$\begin{cases} f_x(x) = k_{x1}x + k_{x3}x^3 \\ f_y(y) = k_{y1}y + k_{y3}y^3. \end{cases}$$
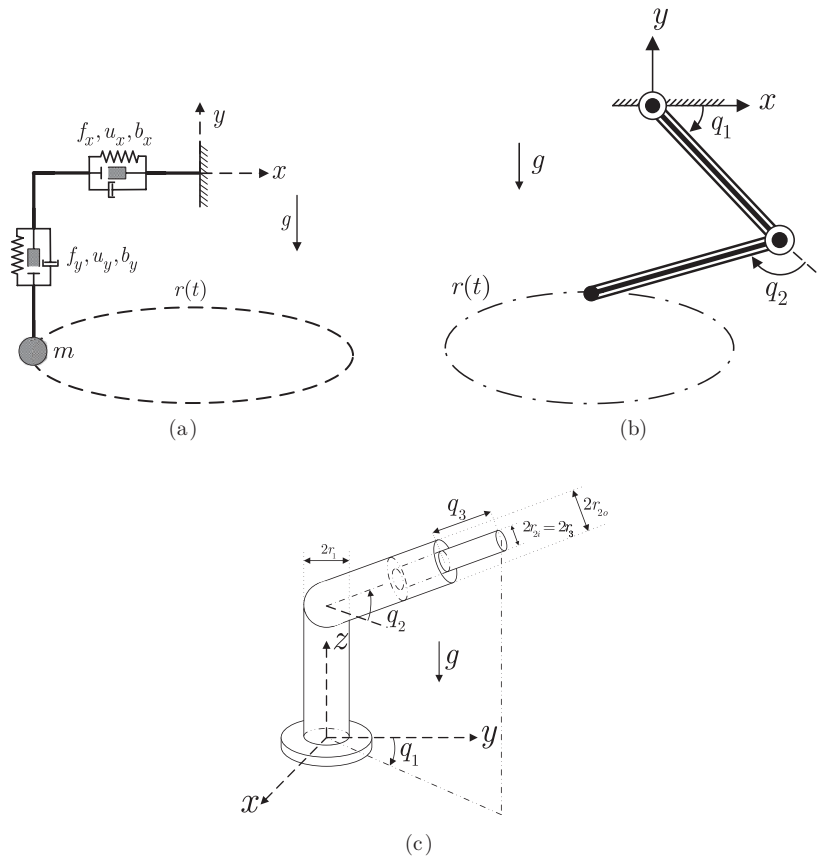
Fig. 1 The case studies setups: (a) A two link manipulator with prismatic joints. (b) A two link manipulator with rotary joints. (c) A three link spherical manipulator (RRP) with two revolute and one prismatic joints.

The desired path for the end-effector is

$$r(t) = \mathbf{R}(\omega t) = \begin{bmatrix} 0.4\sin(\omega t) \\ 0.2\cos(\omega t) - 0.4 \end{bmatrix}.$$

Augmenting the free parameters in vector $\mathbf{z}$, we have

$$\mathbf{z} = \begin{bmatrix} k_{x1}, k_{x3}, k_{y1}, k_{y3}, \omega \end{bmatrix}^T.$$

Using Eq. (8), we obtain the cost function as

$$W(\mathbf{z}) = \frac{\pi}{5}\omega^4 m^2 + \frac{\pi\omega^2}{25}(4b_x^2 + b_y^2) - \frac{\pi\omega^2 m}{1250}(400k_{x1} + 48k_{x3} + 100k_{y1} + 51k_{y3})$$

$$- \frac{\pi}{125}(200gk_{y1}m + 44gk_{y3}m) + \frac{9\pi}{25}(k_{y1}^2 + \frac{227}{450}k_{y1}k_{y3} + \frac{1103}{15,000}k_{y3}^2)$$

$$+ \frac{4\pi}{25}(k_{x1}^2 + \frac{6}{25}k_{x1}k_{x3} + \frac{2}{125}k_{x3}^2) + 2\pi g^2 m^2. \tag{10}$$

Solving Eq. (9) results in $k_{x1}^* = m\omega^{*2}$, $k_{x3}^* = 0$, $k_{y1}^* = \frac{m}{227}(1120g - 171\omega^{*2})$, and $k_{y3}^* = \frac{m}{227}(800\omega^{*2} - 2000g)$; where the optimum frequency is

$$\omega^* = \sqrt{1000gm^2 - 5540b_x^2 - 1385b_y^2}/20m.$$

Table I. The optimum parameters and the minimum value of
the cost functions for linear and cubic basis functions.

	Linear and cubic	Linear	Cubic
ω^*	2.68	4.71	5.584
(k_{x1}^*, k_{x3}^*)	(1.43 , 0.00)	(4.43 , −)	(− , 46.875)
(k_{y1}^*, k_{y3}^*)	(7.03 , −9.99)	(4.93 , −)	(− , 18.104)
W^*	0.39	0.59	5.504
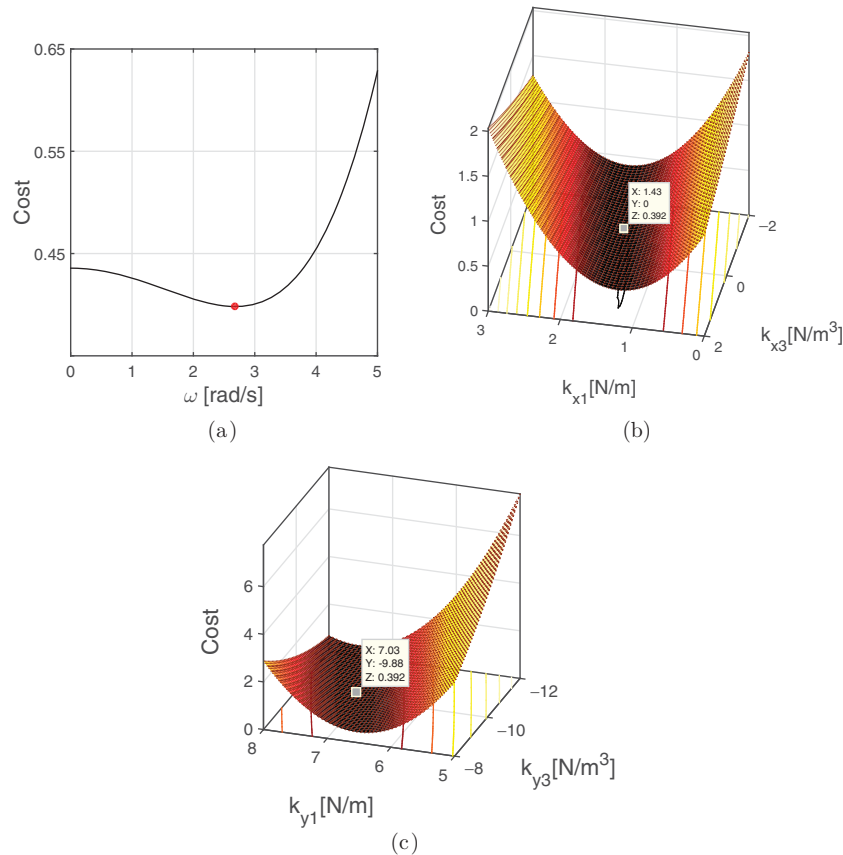
Fig. 2 Validation of the results through search in the parameter space of the 2-DOF prismatic manipulator case. The cost function is plotted vs.: (a) the frequency when the optimum compliances are considered in the joints. (b/c) The compliance coefficients at the first/second joint when the optimum compliance is placed at the other joint and the task is performed at the optimum frequency.

In order to have a deeper inspection, suppose $b_x = b_y = b$. Hence, the necessary condition for the existence of an optimum frequency is $b < m\sqrt{(1000/6925)g}$ which results in $0 < \omega^* \leqslant \sqrt{2.5g}$.

To study the obtained results numerically, suppose $m = 0.2$ kg, $b_x = b_y = 0.2$ Ns/m, and $g = 9.8$ m/s^2. The calculations are performed first using two basis functions (linear and cubic) for the compliance forces and then are repeated with only one of them. The results are presented in Table I.

The results show the importance of having linear compliance in this example. That is, in case of cubic-only compliance, the cost is almost 10 times higher. Having both linear and cubic compliances at the same time results in the lowest cost at the expense of about two times slower motion. Nevertheless, linear-only compliance has the best outcome in terms of COT; i.e., fast motion at low cost. To validate the obtained results, the cost function and the optimum parameters are illustrated in Fig. 2 using a numerical approach. Obviously, the numerically obtained optimum parameters confirm the analytical ones.

4.2. 2-DOF manipulator with revolute joints

Consider a two-link planar manipulator in the vertical plane with linear compliant revolute joints (Fig. 1b). In this setup, a parallel linear spring is considered in each joint with stiffness coefficients $k_i; i = 1, 2$. In addition, the damping coefficient in each joint is $b_i = b \geqslant 0; i = 1, 2$. The length, the width, and the mass of each link are $l = 0.3$ m, $d = 0.04$ m, and $m = 0.5$ kg, respectively. This manipulator can play the role of a swing leg in a locomotor robot. The manipulator's dynamical equations are presented in Appendix C. Considering $\phi_1 = \mathbf{q}_1$ and $\phi_2 = \mathbf{q}_2$, the compliance forces are as follows:

$$\begin{cases} f_1 = k_1 \mathbf{q}_1 \\ f_2 = k_2 \mathbf{q}_2. \end{cases}$$

The desired path for the end-effector is

$$r(t) = \mathbf{R}(\omega t) = \begin{bmatrix} 0.3A \sin(\omega t) - 0.1 \\ 0.1A \cos(\omega t) - 0.4 \end{bmatrix},$$

where A is the amplitude scaling factor. Here, we set $A = 1$; see Section 5.2 for some other cases. According to Definition 3, there are countable mappings for the inverse kinematics. Here, the elbow-up solution in two-link manipulators is chosen (Fig. 1); see Section 5.1 for analyzing the elbow-down solution. Using Eq. (8), we calculate the cost function as

$$W = 0.002067\omega^4 + (-0.05233k_1 + 0.01170k_2 - 0.1088 + 0.7158b^2)\omega^2$$

$$+ 2.048 + 0.9002k_1 + 1.370k_2 + 1.617k_1^2 + 1.961k_2^2.$$

Augmenting the free parameters in vector $\mathbf{z}$, we have

$$\mathbf{z} = [k_1, k_2, \omega]^T.$$

Based on Eq. (9), the optimum parameters are obtained as $k_1^* = -0.2784 + 0.01618\omega^{*2}$, and $k_2^* = -0.3492 - 0.0029\omega^{*2}$; where the optimum frequency is

$$\omega^* = 14.83\sqrt{-b^2 + 0.137}.$$

Hence, $b < 0.3708$ is the condition that implies a non-zero optimum frequency. Depending on the damper value, we have $0 < \omega^* \leqslant 5.49$ and $W^* = -78.8\,b^4 + 21.637\,b^2 + 0.1979$. For instance, for $b = 0.1$ Nms/rad, we have $k_1^* = 0.1735$ Nm/rad, $k_2^* = -0.4302$ Nm/rad, $\omega^* = 5.28$ rad/s, and $W^* = 0.4064$. To validate the obtained results, the cost function and the optimum parameters are illustrated in Fig. 3 using a numerical approach. Obviously, the numerically obtained optimum parameters confirm the analytical ones.

4.3. RRP manipulator with a 3D task

Consider a three-link RRP manipulator with compliant joints (Fig. 1). In this robot, a multi-basis compliance structure (linear and cubic) is considered in each joint with stiffness coefficients of k_{i1}, k_{i3}, $i = 1, 2, 3$. In addition, the damping coefficients in the revolute and the prismatic joints are b_r and b_p, respectively. The first and the third links are assumed to be a solid cylinders with radius of r_1 and r_3, respectively. Also, the second link is assumed to be a thick-walled cylindrical tube with inner radius of r_{2i} and outer radius of r_{2o}. The length and the mass of each link are $l_i; i = 1, 2, 3$ and $m_i; i = 1, 2, 3$, respectively. The parameters' values are presented in Table II and the manipulator's dynamical equations are presented in Appendix D. Considering $\phi_{11} = \mathbf{q}_1, \phi_{13} = \mathbf{q}_1^3$, $\phi_{21} = \mathbf{q}_2, \phi_{23} = \mathbf{q}_2^3, \phi_{31} = \mathbf{q}_3$, and $\phi_{33} = \mathbf{q}_3^3$, the compliance forces are calculated as follows:

$$\begin{cases} f_1(\mathbf{q}_1) = k_{11}\mathbf{q}_1 + k_{13}\mathbf{q}_1^3 \\ f_2(\mathbf{q}_2) = k_{21}\mathbf{q}_2 + k_{23}\mathbf{q}_2^3 \\ f_3(\mathbf{q}_3) = k_{31}\mathbf{q}_3 + k_{33}\mathbf{q}_3^3. \end{cases}$$
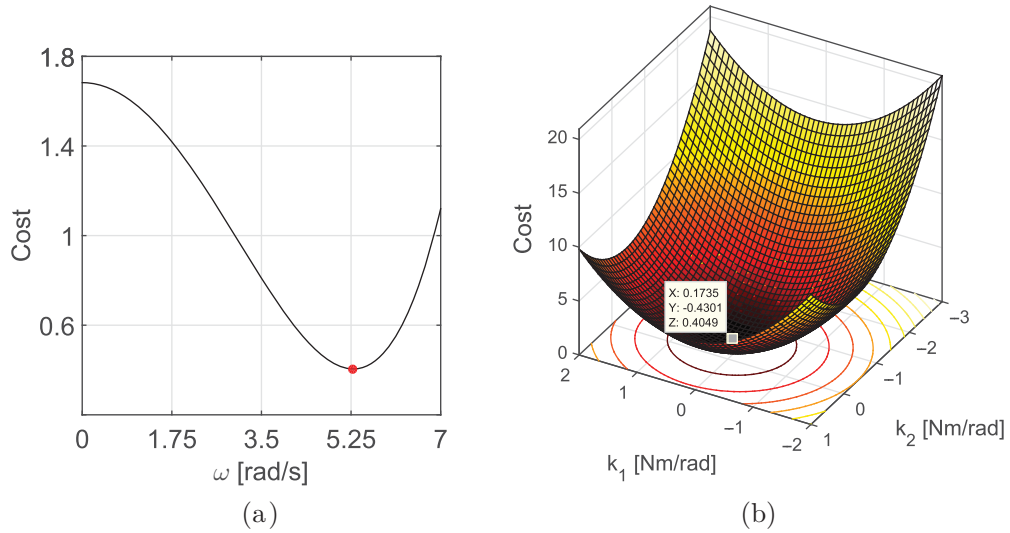
Fig. 3 Validation of the results through search in the parameter space of the 2-DOF revolute manipulator case. The cost function is plotted vs.: (a) the frequency when the optimum compliances are considered in the joints. (b) The compliance coefficients at the first and the second joints when the task is performed at the optimum frequency.
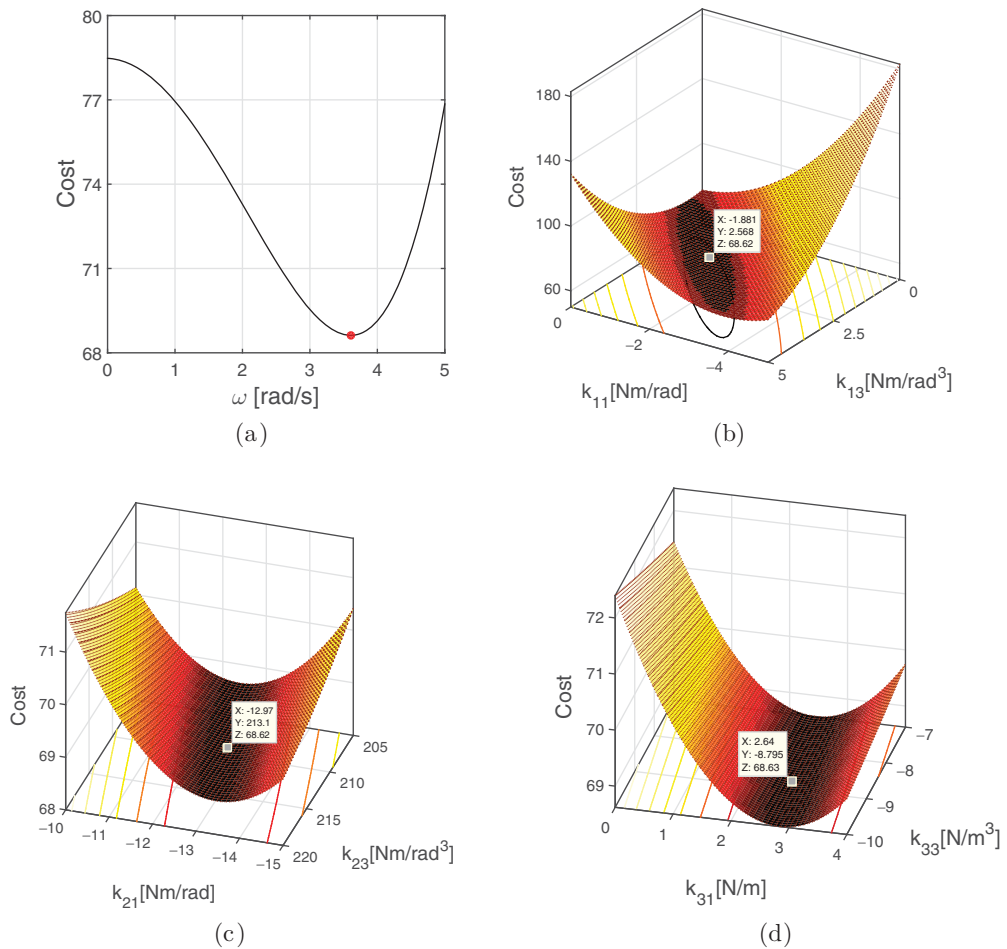
Fig. 4 Validation of the results through search in the parameter space of the 3-DOF RRP manipulator case. The cost function is plotted vs.: (a) the frequency when the optimum compliances are considered in the joints. (b/c/d) The compliance coefficients at the first/second/third joint when the optimum compliances are considered at the other joints and the task is performed at the optimum frequency.

Table II. The RRP robot's parameters.

Parameter	Nominal value	Parameter	Nominal value
r_1, r_{2o}	10 cm	r_3, r_{2i}	8 cm
l_1	1 m	m_1	1 kg
l_2, l_3	0.5 m	m_2, m_3	0.5 kg

Table III. The optimum parameters and the minimum value of the cost functions for linear and cubic basis functions.

	Linear and cubic	Linear	Cubic
ω^*	3.6061	3.0524	3.6376
(k_{11}^*, k_{13}^*)	(1.88, 0.567)	(0.1458, –)	(–, 0.5307)
(k_{21}^*, k_{23}^*)	(−12.96, −213.07)	(1.5112, –)	(–, 64.353)
(k_{31}^*, k_{33}^*)	(2.68, −8.79)	(0.8630, –)	(–, 9.9514)
W^*	68.62	84.28	78.96

The desired path for the end-effector is

$$\begin{cases} x_r = 0.5 + 0.2\cos(\omega t) \\ y_r = 0.5 + 0.2\sin(\omega t) \\ z_r = 1 + 0.2\sin(\omega t). \end{cases}$$

Augmenting the free parameters in vector $\mathbf{z}$, we have

$$\mathbf{z} = [k_{11}, k_{13}, k_{21}, k_{23}, k_{31}, k_{33}, \omega].$$

Using Eq. (8), we obtain the cost function as

$$\begin{aligned} W(\mathbf{z}) &= 0.0570\omega^4 + 0.0023(b_r - b_p)\omega^3 + (-0.1296k_{11} - 0.2477k_{13} \\ &\quad - 0.0802k_{21} - 0.0053k_{23} - 0.1746k_{31} - 0.0269k_{33} + 0.1231b_p^2 \\ &\quad + 0.5465b_r^2 - 0.7607)\omega^2 + 1.1939(b_r - b_p)\omega + 6.7154k_{11}k_{13} \\ &\quad + 0.0368k_{21}k_{23} + 0.1206k_{31}k_{33} + 4.1357k_{11}^2 + 0.4680k_{31}^2 + 0.2606k_{21}^2 \\ &\quad + 0.0016k_{23}^2 + 3.0869k_{13}^2 + 0.0088k_{33}^2 - 0.0408k_{21} - 0.1358k_{23} \\ &\quad + 0.8181k_{31} + 0.1808k_{33} + 87.7369. \end{aligned}$$

Based on Eq. (9), the optimum parameters are $k_{11}^* = -0.1446\omega^{*2}$, $k_{13}^* = 0.1974\omega^{*2}$, $k_{21}^* = -15.5193 + 0.1964\omega^{*2}$, $k_{23}^* = 220.9104 - 0.6026\omega^{*2}$, $k_{31}^* = 3.8387 - 0.0887\omega^{*2}$, and $k_{33}^* = -36.5770 + 2.1364\omega^{*2}$. Where the optimum frequency is the positive real root of the following equation:

$$\begin{aligned} & 0.0586\omega^3 + 0.0069(b_r - b_p)\omega^2 \\ & + (1.0930b_r^2 + 0.2462b_p^2 - 0.7463)\omega + 1.1939(b_r - b_p) = 0. \end{aligned}$$

Considering $b_p = 0.2$ Ns/m and $b_r = 0.1$ Nms/rad, we have $\omega^* = 3.6061$ rad/s. Same as in the first case study, the optimum parameters for one and two basis functions are reported in Table III.

Here, in contrast with the first case study, the cubic basis function is more effective in the cost function minimization in comparison with the linear one. In addition, the optimum frequency in case of using only cubic basis function is almost equal to the optimum frequency in case of using both linear and cubic bases. The results indicate that adding the linear part affects the cost function but does not have a significant effect on the optimum frequency. To validate the obtained results in the case of using both basis functions, the cost function and the optimum parameters are illustrated in

Table IV. The optimum parameters and the minimum value of the cost
functions in different configurations.

	W^*	ω^*	k_1^*	k_2^*
Elbow-up	0.1979	5.4891	0.2091	−0.4394
Elbow-down	0.2139	3.8866	−0.5371	−0.2389

Fig. 4 using a numerical approach. Obviously, the numerically obtained optimum parameters confirm the analytical ones.

4.4. Effects of unmodeled dynamics

In order to check the effects of unmodeled dynamics on the results, we compute the sensitivity factor presented in Section 3.4 for variations in the damping coefficients. In the first case study (Section 4.1), with assumption of 10% deviation in the damping coefficients, we have $S(b_{x0}) \simeq 25\%$ and $S(b_{y0}) \simeq 6.2\%$. This implies that the horizontal damper must be identified or constructed more precise than the vertical one in order to be as energy efficient as the optimization suggests. Similarly, in the second case study (Section 4.2), we have $S(b_0) \simeq 10\%$ which means that 10% error in the nominal value of damping coefficients does not lead to a drastic change in the optimal value of the cost function. Also, in the third case study (Section 4.3), we have $S(b_{p0}) \simeq 0.11\%$ and $S(b_{r0}) \simeq 0.08\%$ for 10% deviation of the damper coefficients from their nominal values. These results show the robustness of the optimum parameters with respect to the deviations of the damping coefficients.

5. Conclusions and Discussions

We proved that for a serial manipulator, the vector of the desired generalized forces/torques to track a reference cyclic trajectory is a linear function of the parallel compliance coefficients and a quadratic function of the task frequency. These properties provided us with a powerful toolbox for analytical and global minimization of any force-based cost function. Accordingly, we demonstrated that, the defined cost function has a quadratic shape with respect to the compliance coefficients and a quartic shape with respect to the task frequency. Using these properties, we presented an analytical method for minimization of energy consumption in cyclic tasks. Our method is based on simultaneous modification and exploitation of the robot's natural dynamics through optimization of the task frequency and the compliance coefficients, installed in parallel with actuators at joints. Therefore, employing this method leads to a drastic reduction in energy consumption by using two complementary means, natural dynamics shaping and exploiting, simultaneously. According to our mathematics, the defined cost function is a function of the robot's dynamical equations, hence, increasing DOFs of the robot highly increases computational complexity.

In the following subsections, we discuss some interesting results achieved in the case studies.

5.1. Effect of pose

Here, we investigate the effects of different inverse kinematics solutions on the optimum compliances and the task frequency in the second case study (Section 4.2). In that case, we studied the elbow-up inverse kinematics solution. If we select the elbow-down solution, the results are $k_1^* = -0.5719 + 0.0023\omega^{*2}$ and $k_2^* = -0.2541 + 0.0010\omega^{*2}$, where the optimum frequency is

$$\omega^* = 13.45\sqrt{-b^2 + 0.0835}.$$

Hence, $b < 0.289$ is the condition to have a non-zero optimum frequency. It means, depending on the damper values, we have $0 < \omega^* \leqslant 3.8866$ and $W^* = -49.09\,b^4 + 8.20\,b^2 + 0.2139$. Clearly, the upper bound on the damper value in the elbow-up configuration is lower than in the elbow-down configuration. The optimum parameters and the minimum value of the cost function for $b = 0$ in both solutions are presented in Table IV.

According to this table, the elbow-up configuration results in lower energy consumption and faster movement. Interestingly, swing legs of walking systems are mostly in the elbow-up configuration.
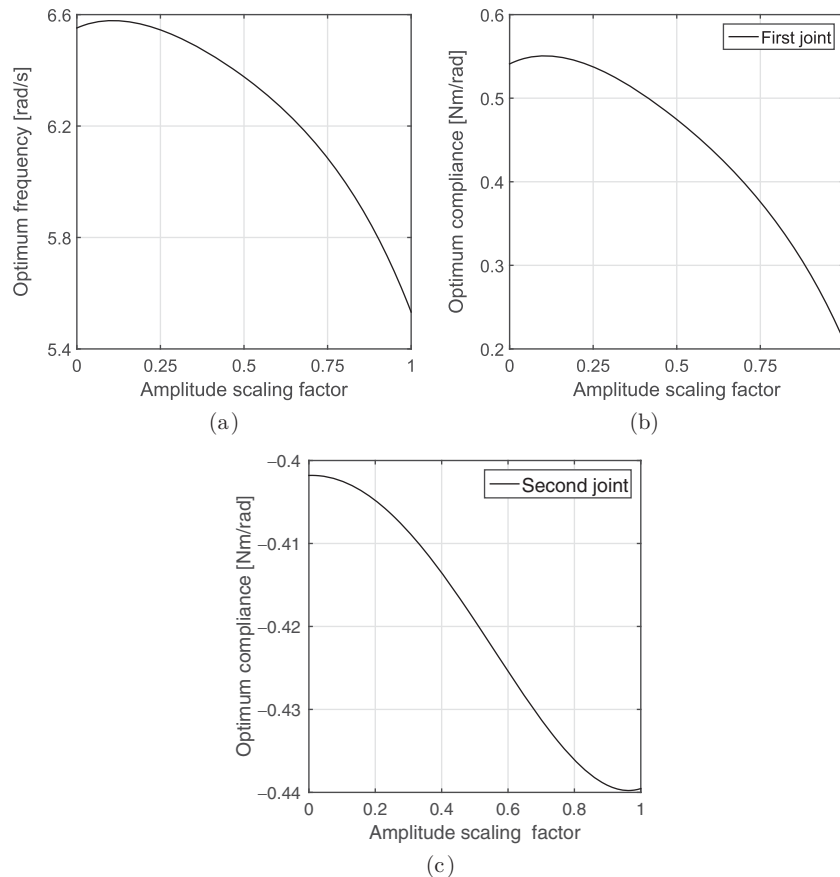
Fig. 5 Effects of the amplitude scaling factor on the optimum compliances and the task frequency.

One of the reasons, besides others, might be to have a lower COT (in legged locomotion, COT is defined as the energy consumed by the robot divided by its forward velocity, which is proportional with the gait frequency).

5.2. Effects of amplitude scaling

In this subsection, we study the effect of task amplitude (A in the second case study Section 4.2) on the optimum parameters for zero damping ($b = 0$); see Fig. 5. The optimum frequency and the first joint's compliance coefficient are inversely correlated with the task amplitude while the second joint's optimum compliance does not change much. In other words, in case of varying task amplitude, the second joint's compliance can be kept constant while the compliance at the first joint and the task frequency require tuning to attain the maximum energy efficiency. Nevertheless, the figure shows that, the robot with a fixed task frequency and compliances at the joints remains almost energy efficient for a small variation in the task amplitude. Note that here, the task amplitude is equivalent to stride length in legged locomotion; see ref. [26] as a structure with coupled frequency-amplitude. Therefore, our results point to the importance of having variable compliance at hip while having constant stiffness at knee suffices.

5.3. Effects of motor's dynamical equations

In the presented approach, the cost function is defined over the actuator's applied torque. However, by means of our mathematics, we can include the effects of motor's dynamics in the optimization process. Assuming permanent magnet DC-motors' dynamical equations, we can define the cost function over

the input voltages of the motors. The dynamical equations of motors are as follows:

$$\mathbf{u}_m - \mathbf{u} = \mathbf{J}_m \ddot{\mathbf{q}} + \mathbf{B}_m \dot{\mathbf{q}}, \tag{11}$$

$$\mathbf{u}_m = \mathbf{K}_T \mathbf{I}_m, \tag{12}$$

$$\mathbf{V}_m = \mathbf{R}_m \mathbf{I}_m + \mathbf{L}_m \dot{\mathbf{I}}_m + \mathbf{K}_v \dot{\mathbf{q}}, \tag{13}$$

where $\mathbf{u}_m = [u_{m1}, u_{m2}, \ldots, u_{mn}]^T$ is the vector of motors' torques, $\mathbf{u} = [u_1, u_2, \ldots, u_n]^T$ is the vector of applied torques to the robot (Eq. (1)), $\mathbf{J}_m = diag(J_{m1}, J_{m2}, \ldots, J_{mn})$ is the rotors' moment of inertia matrix, $\mathbf{B}_m = diag(B_{m1}, B_{m2}, \ldots, B_{mn})$ is the damping coefficients matrix, $\mathbf{K}_T = diag(K_{T1}, K_{T2}, \ldots, K_{Tn})$ is the torque constant matrix, $\mathbf{I}_m = [I_{m1}, I_{m2}, \ldots, I_{mn}]^T$ is the input currents vector, $\mathbf{R}_m = diag(R_{m1}, R_{m2}, \ldots, R_{mn})$ is the matrix of terminal resistance, $\mathbf{L}_m = diag(L_{m1}, L_{m2}, \ldots, L_{mn})$ is the matrix of terminal inductance, $\mathbf{K}_v = diag(K_{v1}, K_{v2}, \ldots, K_{vn})$ is the back emf constant matrix, and $\mathbf{V}_m = [V_{m1}, V_{m2}, \ldots, V_{mn}]^T$ is the vector of motors' terminal voltages. Substituting Eqs. (1) and (12) into Eq. (11), we have

$$\mathbf{K}_T \mathbf{I}_m = (\mathbf{M}(\mathbf{q}) + \mathbf{J}_m)\ddot{\mathbf{q}} + (\mathbf{C}(\mathbf{q}, \dot{\mathbf{q}}) + \mathbf{B}_m + \mathbf{B})\dot{\mathbf{q}} + \mathbf{G}(\mathbf{q}) + \mathbf{F}(\mathbf{q}). \tag{14}$$

Taking first time derivative of Eq. (14), we have

$$\mathbf{K}_T \dot{\mathbf{I}}_m = (\mathbf{M} + \mathbf{J}_m)\dddot{\mathbf{q}} + \dot{\mathbf{M}}_m \ddot{\mathbf{q}} + (\mathbf{C} + \mathbf{B}_m + \mathbf{B})\ddot{\mathbf{q}} + \dot{\mathbf{C}}\dot{\mathbf{q}} + \dot{\mathbf{G}} + \dot{\mathbf{F}}. \tag{15}$$

Substituting $\dot{\mathbf{I}}_m$ from Eq. (13) and $\mathbf{I}_m$ from Eq. (14) into Eq. (15), we obtain the required voltage of the motors as

$$\begin{aligned}
\mathbf{V}_m &= \mathbf{L}_m \mathbf{K}_T^{-1}((\mathbf{M} + \mathbf{J}_m)\dddot{\mathbf{q}} + (\dot{\mathbf{M}} + \mathbf{C} + \mathbf{B}_m + \mathbf{B})\ddot{\mathbf{q}} + \dot{\mathbf{C}}\dot{\mathbf{q}} + \dot{\mathbf{G}} + \dot{\mathbf{F}}) \\
&\quad + \mathbf{K}_v \dot{\mathbf{q}} + \mathbf{R}_m \mathbf{K}_T^{-1}((\mathbf{M} + \mathbf{J}_m)\ddot{\mathbf{q}} + (\mathbf{C} + \mathbf{B}_m + \mathbf{B})\dot{\mathbf{q}} + \mathbf{G}(\mathbf{q}) + \mathbf{F}(\mathbf{q})).
\end{aligned}$$

Substituting $\mathbf{q}^{(k)} = \mathbf{q}_r^{(k)}(\omega t)$; $k = 0, 1, 2, 3$, we can find the desired motor voltages for the robot to perform the task. Henceforth, we can easily transform the desired motor voltages similar to what we did in Eq. (6). Interestingly, in this case, the transformed motors' voltage vector is cubic with respect to the task frequency and is linear with respect to the compliance coefficients. Now we can redefine the cost function as the total energy consumed by the DC-motors during one cycle as

$$W = \int_0^{2\pi} \mathbf{V}_m^T N \mathbf{V}_m \mathrm{d}\theta = \omega \int_0^{2\pi/\omega} \mathbf{V}_m^T N \mathbf{V}_m \mathrm{d}t.$$

This cost function is hexic with respect to the task frequency and is quadratic with respect to the compliance coefficients. Increasing the order of frequency in the cost function can be explained by increasing the order of differential equations by adding dynamical equations of DC-motors.

To consider the speed limitation of DC-motors, we have to impose an upper bound on the optimum frequency. Hence, in this case, the optimum parameters ($\mathbf{z}^*$) could be obtained by solving the following optimization problem:

$$\begin{aligned}
\mathbf{z}^* &= \arg \min_{\mathbf{z}} W(\mathbf{z}) \,;\, \mathbf{z} = [k_{11}, \ldots, k_{1m}, \ldots, k_{n1}, \ldots, k_{nm}, \omega]^T \\
&\text{subject to} : 0 \le \omega \le \omega_{\max},
\end{aligned}$$

where $\omega_{\max}$ is the maximum permissible speed for the motors.

References

1. F. Bauer, U. Römer, A. Fidlin and W. Seemann, "Optimization of energy efficiency of walking bipedal robots by use of elastic couplings in the form of mechanical springs," *Nonlinear Dyn.* **83**, 1275–1301 (2016).
2. H. J. Bidgoly, M. N. Ahmadabadi and M. R. Zakerzadeh, "Design and Modeling of a Compact Rotational Nonlinear Spring," *Proceedings of the IEEE/RSJ International Conference on Intelligent Robots and Systems (IROS)*, IEEE, Daejeon, Korea (2016) pp. 4356–4361.
3. J. Buchli, F. Iida and A. J. Ijspeert, "Finding Resonance: Adaptive Frequency Oscillators for Dynamic Legged Locomotion," *Proceedings of the IEEE/RSJ International Conference of Intelligent Robots and Systems,* IEEE, Beijing, China (2006) pp. 3903–3909.
4. S. Collins, A. Ruina, R. Tedrake and M. Wisse, "Efficient bipedal robots based on passive-dynamic walkers," *Science* **307**, 1082–1085 (2005).
5. S. Cotton, I. M. C. Olaru, M. Bellman, T. Van der Ven, J. Godowski and J. Pratt, "Fastrunner: A Fast, Efficient and Robust Bipedal Robot. Concept and Planar Simulation," *Proceedings of the IEEE International Conference on Robotics and Automation (ICRA),* IEEE, St. Paul, MN, USA (2012) pp. 2358–2364.
6. M. Grimmer, M. Eslamy, S. Gliech and A. Seyfarth, "A Comparison of Parallel-and Series Elastic Elements in an Actuator for Mimicking Human Ankle Joint in Walking and Running," *Proceedings of the 2012 IEEE International Conference on Robotics and Automation (ICRA),* IEEE, St. Paul, MN, USA (2012) pp. 2463–2470.
7. A. J. Ijspeert, "Central pattern generators for locomotion control in animals and robots: A review," *Neural Netw.* **21**, 642–653 (2008).
8. A. Jafari, N. G. Tsagarakis and D. G. Caldwell, "A novel intrinsically energy efficient actuator with adjustable stiffness (awas)," *IEEE/ASME Trans. Mechatron.* **18**, 355–365 (2013).
9. M. Khoramshahi, R. Nasiri, A. Ijspeert and M. N. Ahmadabadi, "Energy Efficient Locomotion with Adaptive Natural Oscillator," *Dynamic Walking 2014*, EPFL-CONF-199765 (2014).
10. M. Khoramshahi, A. Parsa, A. Ijspeert and M. N. Ahmadabadi, "Natural Dynamics Modification for Energy Efficiency: A Data Driven Parallel Compliance Design Method,"*Proceedings of the International Conference on Robotics and Automation (ICRA)*, IEEE, Hong Kong, China (2014) pp. 2412–2417.
11. S. Martínez, C. A. Monje, A. Jardón, P. Pierro, C. Balaguer and D. Munoz, "Teo: Full-size humanoid robot design powered by a fuel cell system," *Cybern. Syst.* **43**, 163–180 (2012).
12. MATLAB (2015-b). Mathworks Inc. http://www.mathworks.com.
13. T. McGeer, "Passive dynamic walking," *Int. J. Robot. Res.* **9**, 62–82 (1990).
14. S. Mozaffari, E. Rekabi, R. Nasiri and M. N. Ahmadabadi, "Design and Modeling of a Novel Multi-Functional Elastic Actuator (MFEA)," *Proceedings of the 4th International Conference on Robotics and Mechatronics (ICROM)*, IEEE, University of Tehran, Tehran, Iran (2016).
15. R. Nasiri, M. Khoramshahi and M. N. Ahmadabadi, "Design of a Nonlinear Adaptive Natural Oscillator: Towards Natural Dynamics Exploitation in Cyclic Tasks," *Proceedings of the IEEE/RSJ International Conference on Intelligent Robots and Systems (IROS)*, IEEE, I Daejeon, Korea (2016) pp. 3653–3658.
16. R. Nasiri, M. Khoramshahi, M. Shushtari and M. N. Ahmadabadi, "Adaptation in variable parallel compliance: Towards energy efficiency in cyclic tasks," *IEEE/ASME Trans. Mechatron.*, IEEE (2016). Available at: http://ieeexplore.ieee.org/document/7778166/.
17. D. Pérez and Y. Quintana, "A survey on the weierstrass approximation theorem," *Divulgaciones Matemáticas* **16**, 231–247 (2008).
18. J. Peters, M. Mistry, F. Udwadia, J. Nakanishi and S. Schaal, "A unifying framework for robot control with redundant dofs," *Auton. Robots* **24**, 1–12 (2008).
19. L. Righetti, J. Buchli and A. J. Ijspeert, "Dynamic hebbian learning in adaptive frequency oscillators," *Phys. D: Nonlinear Phenom.* **216**, 269–281 (2006).
20. S. Schaal, J. Peters, J. Nakanishi and A. Ijspeert, "Learning Movement Primitives," *Proceedings of the 11th International Symposium Robotics Research*, Springer (2005) pp. 561–572.
21. A. Schepelmann, K. A. Geberth and H. Geyer, "Compact Nonlinear Springs with User Defined Torque-Deflection Profiles for Series Elastic Actuators," *Proceedings of the IEEE International Conference on Robotics and Automation (ICRA)*, IEEE, Hong Kong, China (2014) pp. 3411–3416.
22. N. Schmit and M. Okada, "Simultaneous Optimization of Robot Trajectory and Nonlinear Springs to Minimize Actuator Torque," *Proceedings of the IEEE International Conference on Robotics and Automation (ICRA)*, IEEE, St. Paul, MN, USA (2012) pp. 2806–2811.
23. Schmit, N. and M. Okada, "Optimal design of nonlinear springs in robot mechanism: simultaneous design of trajectory and spring force profiles," *Adv. Robot.* **27**, 33–46 (2013).
24. S. Seok, A. Wang, M. Y. Chuah, D. Otten, J. Lang and S. Kim, "Design Principles for Highly Efficient Quadrupeds and Implementation on the Mit Cheetah Robot," *Proceedings of the IEEE International Conference on Robotics and Automation (ICRA),* IEEE, Karlsruhe, Germany (2013) pp. 3307–3312.
25. N. Shafii, N. Lau and L. P. Reis, "Generalized Learning to Create an Energy Efficient zmp-Based Walking," *Robocup 2014: Robot World Cup xviii*, Springer (2015) pp. 583–595.
26. M. Shakiba, M. H. Shadmehr, O. Mohseni, R. Nasiri and M. N. Ahmadabadi, "An Adaptable Cat-Inspired Leg Design with Frequency-Amplitude Coupling," *Proceedings of the 4th RSI International Conference on Robotics and Mechatronics (ICROM)*, IEEE, University of Tehran, Tehran, Iran (2016).
27. H.-K. Shin and B. K. Kim, "Energy-efficient gait planning and control for biped robots utilizing the allowable zmp region," *IEEE Trans. Robot.* **30**, 986–993 (2014).

28. M. W. Spong, S. Hutchinson and M. Vidyasagar, *Robot Modeling and Control*, vol. 3 (Wiley, New York, 2006).
29. K. Sreenath, H.-W. Park, I. Poulakakis and J. W. Grizzle, "A compliant hybrid zero dynamics controller for stable, efficient and fast bipedal walking on mabel," *Int. J. Robot. Res.* **30**, 1170–1193 (2011).
30. N. G. Tsagarakis, Z. Li, J. Saglia and D. G. Caldwell, "The Design of the Lower Body of the Compliant Humanoid robot Ccub," *Proceedings of the IEEE International Conference on Robotics and Automation (ICRA),* IEEE, International Conference Center, Shanghai, China (2011) pp. 2035–2040.
31. M. Uemura, H. Goya and S. Kawamura, "Motion control with stiffness adaptation for torque minimization in multijoint robots," *IEEE Trans. Robot.* **30**, 352–364 (2014).
32. R. Van Ham, B. Vanderborght, M. Van Damme, B. Verrelst and D. Lefeber, "Maccepa, the mechanically adjustable compliance and controllable equilibrium position actuator: Design and implementation in a biped robot," *Robot. Auton. Syst.* **55**, 761–768 (2007).
33. B. Vanderborght, A. Albu-Schaeffer, A. Bicchi, E. Burdet, D. G. Caldwell, R. Carloni, M. Catalano, O. Eiberger, W. Friedl and G. Ganesh, "Variable impedance actuators: A review," *Robot. Auton. Syst.* **61**, 1601–1614 (2013).
34. L. C. Visser, R. Carloni, R. Unal and S. Stramigioli, "Modeling and Design of Energy Efficient Variable Stiffness Actuators," *Proceedings of the IEEE International Conference on Robotics and Automation (ICRA),* IEEE, Egan Convention Center, Anchorage, AK, USA (2010) pp. 3273–3278.

Appendix A. Desired Forces/Torques Extraction

Based on [28, pp. 202], we have

$$\mathbf{C}_{ij}(\mathbf{q}_r, \dot{\mathbf{q}}_r) = 0.5 \sum_{k=1}^{n} \left(\frac{\partial \mathbf{M}_{ij}(\mathbf{q}_r)}{\partial \mathbf{q}_{r_j}} + \frac{\partial \mathbf{M}_{ik}(\mathbf{q}_r)}{\partial \mathbf{q}_{r_j}} - \frac{\partial \mathbf{M}_{kj}(\mathbf{q}_r)}{\partial \mathbf{q}_{r_i}} \right) \dot{\mathbf{q}}_{r_k}. \tag{A1}$$

On the other hand, we have

$$\dot{\mathbf{q}}_r = \frac{\partial \mathbf{q}_r(\omega t)}{\partial (\omega t)} \frac{\mathrm{d}(\omega t)}{\mathrm{d}t} = \omega \mathbf{q}'_r(\omega t), \tag{A2}$$

$$\ddot{\mathbf{q}}_r = \frac{\partial^2 \mathbf{q}_r(\omega t)}{\partial (\omega t)^2} \left(\frac{\mathrm{d}(\omega t)}{\mathrm{d}t} \right)^2 = \omega^2 \mathbf{q}''_r(\omega t). \tag{A3}$$

Substituting Eqs. (A3), (A2), and (A1) into Eq. (5), we have

$$\mathbf{u}_i = \omega^2 \psi_i + b_i \omega \mathbf{q}'_{r_i} + \mathbf{G}_i(\mathbf{q}_r) + \mathbf{F}_{c_i}(\mathbf{q}_r),$$

where $\psi_i(\omega t)$ is

$$\psi_i(\omega t) = \sum_{j=1}^{n} ((\mathbf{M}_{ij}(\mathbf{q}_r)\mathbf{q}''_{r_j})$$

$$+ \frac{1}{2} \mathbf{q}'_{r_j}(\omega t) \sum_{k=1}^{n} (\frac{\partial \mathbf{M}_{ij}(\mathbf{q}_r)}{\partial \mathbf{q}_{r_j}} + \frac{\partial \mathbf{M}_{ik}(\mathbf{q}_r)}{\partial \mathbf{q}_{r_j}} - \frac{\partial \mathbf{M}_{kj}(\mathbf{q}_r)}{\partial \mathbf{q}_{r_i}})\mathbf{q}'_{r_k}).$$

Hence, the vector of desired forces/torques is

$$\mathbf{u} = \omega^2 \Psi(\omega t) + \omega \mathbf{B}\mathbf{q}'_r(\omega t) + \mathbf{G}(\mathbf{q}_r(\omega t)) + \mathbf{F}_c(\mathbf{q}_r(\omega t)),$$

where $\Psi(\omega t) = [\psi_1(\omega t), \psi_2(\omega t), \ldots, \psi_n(\omega t)]^T$.

Appendix B. Cost Function Coefficients

$$\alpha_0 = \omega \int_0^{\frac{2\pi}{\omega}} \mathbf{G}^T \mathbf{N} \mathbf{G} \mathrm{d}t \; , \;\; \alpha_1 = 2\omega \int_0^{\frac{2\pi}{\omega}} \mathbf{q}'^T_r \mathbf{B} \mathbf{N} \mathbf{G}(\omega t) \mathrm{d}t,$$

$$\alpha_2 = \omega \int_0^{\frac{2\pi}{\omega}} \left(2\Psi^T(\omega t) \mathbf{N} \mathbf{G}(\omega t) + \mathbf{q}'^T_r \mathbf{B} \mathbf{N} \mathbf{B} \mathbf{q}'_r \right) \mathrm{d}t,$$

$$\alpha_3 = \omega \int_0^{\frac{2\pi}{\omega}} 2\Psi^T(\omega t) \mathbf{N} \mathbf{B} \mathbf{q}'_r \mathrm{d}t \; , \;\; \alpha_4 = \omega \int_0^{\frac{2\pi}{\omega}} \Psi^T(\omega t) \mathbf{N} \Psi(\omega t) \mathrm{d}t,$$

$$\gamma_{ij} = \omega \int_0^{\frac{2\pi}{\omega}} (2\phi_{ij} \sum_{l=1}^n \psi_l \mathbf{N}_{li}) \mathrm{d}t \; , \;\; \zeta_{ijls} = \omega \int_0^{\frac{2\pi}{\omega}} \phi_{ij} \phi_{ls} \mathbf{N}_{il} \mathrm{d}t,$$

$$\lambda_{ij} = \omega \int_0^{\frac{2\pi}{\omega}} (2\phi_{ij} \sum_{l=1}^n \mathbf{q}'_{r_l} b_l \mathbf{N}_{li}) \mathrm{d}t \; , \;\; \xi_{ij} = \omega \int_0^{\frac{2\pi}{\omega}} (2\phi_{ij} \sum_{l=1}^n \mathbf{G}_l \mathbf{N}_{li}) \mathrm{d}t.$$

Appendix C. Dynamical Parameter of the 2-DOF Revolute Manipulator

$$M_{11} = l_1 l_2 m_2 \cos(q_2(t)) + ((d^2 + 12l_2^2 + 4l_2^2)m_2 + m_1(d^2 + 4l_1^2))/12,$$
$$M_{12} = m_2(6l_1 l_2 \cos(q_2(t)) + d^2 + 4l_2^2)/12,$$
$$M_{21} = m_2(6l_1 l_2 \cos(q_2(t)) + d^2 + 4l_2^2)/12 \; , \;\; M_{22} = m_2(d^2 + 4l_2^2)/12,$$
$$C_{11} = 0 \; , \;\; C_{22} = 0,$$
$$C_{12} = -\sin(q_2(t))l_1 l_2 m_2(\dot{q}_2(t) + 2\dot{q}_1(t))/2,$$
$$C_{21} = \sin(q_2(t))\dot{q}_1(t)l_2 m_2 l_1/2,$$
$$G_1 = (m_2 l_2 \cos(q_1(t) + q_2(t)) + l_1 \cos(q_1(t))(m_1 + 2m_2))g/2,$$
$$G_2 = m_2 g l_2 \cos(q_1(t) + q_2(t))/2.$$

Appendix D. Dynamical Parameters of the RRP spherical Manipulator

$$\begin{aligned}
M_{11} &= (12q_3(t)^2 m_3 + 24m_3(l_2 - l_3/2)q_3(t) + \left(12l_2^2 - 12l_2 l_3 + 4l_3^2 - 3r_3^2\right)m_3 \\
&\quad - 3m_2\left(r_{2o}^2 + r_{2i}^2 - 4l_2^2/3\right))\cos(2q_2(t))/24 + q_3(t)^2 m_3/2 + m_3(l_2 - l_3/2)q_3(t) \\
&\quad + (12l_2^2 - 12l_2 l_3 + 4l_3^2 + 9r_3^2)m_3/24 + l_2^2 m_2/6 + (9r_{2i}^2 + 9r_{2o}^2)m_2/24 \\
&\quad + m_1(l_1^2 + 3r_1^2)/12 \; , \;\; M_{22} = q_3(t)^2 m_3 + 2m_3(l_2 - l_3/2)q_3(t) \\
&\quad + (12l_2^2 - 12l_2 l_3 + 4l_3^2 + 3r_3^2)m_3/12 + m_2(l_2^2 + 3r_{2i}^2/4 + 3r_{2o}^2/4)/3,
\end{aligned}$$

$$M_{33} = m_3 \; , \;\; M_{12} = M_{23} = M_{13} = 0 \; , \;\; C_{11} = 0,$$

$$\begin{aligned}
C_{12} &= -\dot{q}_1(t)(q_3(t)^2 m_3 + 2m_3(l_2 - l_3/2)q_3(t) \\
&\quad + (l_2^2 - l_2 l_3 + l_3^2/3 - r_3^2/4)m_3 + m_2(l_2^2 - 3r_{2i}^2/4 - 3r_{2o}^2/4)/3)\sin(2q_2(t)),
\end{aligned}$$

$$C_{13} = m_3 \dot{q}_1(t)(q_3(t) + l_2 - l_3/2)(\cos(2q_2(t)) + 1),$$

$$\begin{aligned}
C_{21} &= \dot{q}_1(t)(q_3(t)^2 m_3 + 2m_3(l_2 - l_3/2)q_3(t) + (l_2^2 - l_2 l_3 + l_3^2/3 - r_3^2/4)m_3 \\
&\quad + m_2(l_2^2 - 3r_{2i}^2/4 - 3r_{2o}^2/4)/3)\sin(2q_2(t))/2,
\end{aligned}$$

$$C_{22} = 0 \ , \ C_{33} = 0 \ , \ C_{23} = \dot{q}_2(t) m_3 \left(2q_3(t) + 2l_2 - l_3 \right),$$

$$C_{31} = -m_3 \, \dot{q}_1(t)(q_3(t) + l_2 - l_3/2)(\cos(2q_2(t)) + 1)/2,$$

$$C_{32} = -\dot{q}_2(t) m_3 (2q_3(t) + 2l_2 - l_3)/2 \ , \ G_1 = 0,$$

$$G_2 = (q_3(t)m_3 + m_3(l_2 - l_3/2) + m_2 l_2/2) \cos(q_2(t)) g, \ G_3 = m_3 \sin(q_2(t)) g.$$